Design and Fabrication of Birdcage Resonators for Low-pressure Plasma Excitation

Karel JURIK [1], Jiri STARY [2], Petr DREXLER [1]

[1] Dept. of Theoretical and Experimental Electrical Engineering, Brno University of Technology, Technická 12, 616 00 Brno, Czech Republic
[2] Dept. of Electrical and Electronic Technology, Brno University of Technology, Technická 10, 616 00 Brno, Czech Republic

{karel.jurik, qestary, drexler}@vut.cz

Submitted October 12, 2022 / Accepted November 24, 2022 / Online first December 20, 2022

Abstract. *This paper presents a design, analysis and optimization of birdcage resonators employed in a novel radio-frequency plasma source. Three resonators were simulated and fabricated. The resonators differ in their design and in the different materials of used dielectric – polyimide and polytetrafluorethylene (PTFE). The resonance frequency of fabricated samples possesses a maximal error of 2.2% compared to the simulated values. The performance in plasma excitation is related to the electrical parameters, while the best performing resonator (PTFE-based) exhibits the maximum real impedance of 644.3 Ω at the resonance frequency and the 799.5 V/m electric field strength. This resonator shows the best power efficiency in a plasma ignition experiment. The resonator ignited the discharge at ca. 1 Pa of ambient air atmosphere with only 0.34 W of input radiofrequency power.*

Keywords

Birdcage resonator, resonance network, plasma source, impedance matching, distributed capacity

1. Introduction

For the very first time, the birdcage resonator was introduced in 1985 by Cecil E. Hayes [1]. The resonators consist of an even number of legs, and capacitors, which may be placed in the middle of the legs (so-called low-pass type, as shown in Fig. 1), between the legs in the endrings (high-pass) and their combination – band-pass type [2].

However, some of the important details of these resonators were not mentioned that time. For instance, the capacitors are mentioned schematically in the original article, where a capacitor in the middle of the legs is shown (see Fig. 1). Later, in an overview article, more details were relieved by the author [3]. The low-pass birdcage was fabricated on a Teflon substrate, with many capacitors in series, which creates the resulting capacitance (Fig. 2).

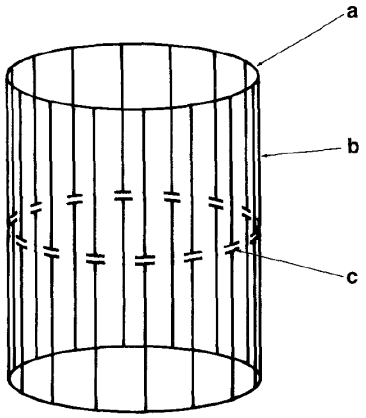

Fig. 1. Low-pass version of a birdcage resonator. Adapted from [1].

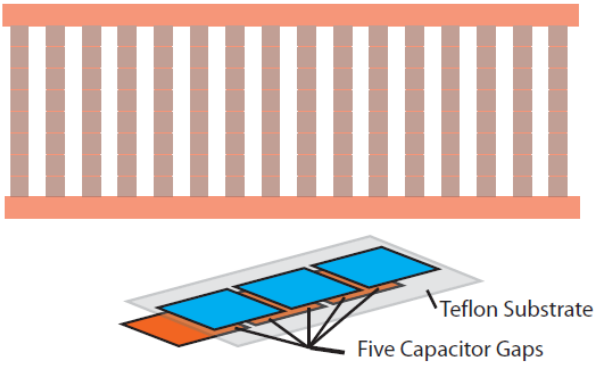

Fig. 2. Design of the birdcage resonator shown in [3].

Originally, the resonators were designed as volume coils for magnetic resonance imaging (MRI) [1]. Since that time, the resonators for MRI were prepared in many variations, using lumped capacitors [4], relying on distributed capacity [5] or by a combination of flexible and rigid substrates with lumped elements [6]. Also, special approaches, e.g., with two overlapping copper/FR-4 structures, to create variable capacity, were published [7].

Although there is plenty of work dealing with birdcage resonators for MRI [8], their application in plasma process-

DOI: 10.13164/re.2023.0044

ing is not examined profoundly yet. There is the work of Ph. Guittienne [9–12] and his colleagues, who employ the birdcage resonators in a plasma source. The presented source utilizes helicon waves excitation, is operating at relatively low frequencies (13.56 MHz) and requires high rf power for its operation (300 W to 10 kW). The birdcage resonator in that source has a diameter of 13 cm and a length of the legs of 15 cm [12].

Plasma ignition in a plasma source with the birdcage resonator at a frequency relevant to today's state-of-the-art MRI devices [13], [14] was not studied up to this moment. Our team have already brought preliminary work on this topic [15], [16]; however, only the electrical properties of the resonators have been studied yet. All types of birdcage resonators possess so-called "fundamental resonance mode", which creates a homogeneous distribution of magnetic field inside their volume. However, the total number of resonance modes, their relative position and the electric field distribution differ for different types.

While all types of resonators are suitable for MRI, where the crucial factor is the distribution and homogeneity of the magnetic field, for plasma processing only the high-pass configuration possesses the correct electric field distribution at the fundamental resonance mode. In plasma processing, the strength and distribution of the electric field are more important. The electrons are accelerated by the electric field, leading to collisions with the gas particles and their ionization. The low-pass resonators create a gap with zero electric field along their axis. The electric fields are shown in Fig. 3 for comparison.

In 2005, Ph. Guittienne employ the birdcage resonator for volume plasma processing. Advantages of specific geometry (called "twisted antenna") were discussed [9]. Later, a possibility to employ a planar resonator, instead of a tubular birdcage design, for plasma excitation was presented. In this work, also the influence of different positions of feeding points is discussed [10].

The phenomenon was recently further studied [17]. If the planar resonator is wrapped in the shape of the birdcage resonator, it possesses the same field distribution at selected resonance modes, which are further dependent on a feeding point position.

The experimental work is discussed in sections below. Section 2 describes the design of the resonators and details of their fabrication. Section 3 describes the characterization of electrical parameters of the resonators (such as their impedance) and its results. Section 4 subsequently describes other components of the final apparatus and the conditions of the experiments. In the same part of the article, the resonators are compared with regard to their performance in plasma excitation. In Sec. 5, aspects of different impedance matching are described and compared.

2. Resonator's Design and Fabrication

Firstly, two resonators were designed employing a flexible two-sided substrate with polytetrafluorethylene (PTFE) dielectric with 127 µm thickness and 18 µm of copper on both sides. The copper-PTFE-copper structure provides the distributed capacity of the resonator. After a preliminary numerical analysis of these two resonators, also a third resonator was created, similar in its design to the better-performing resonator (see results in Sec. 3), however, the resonator was based on a substrate with 35 µm thick polyimide (PI) dielectric with 35 µm both-sided copper. All these resonators were of the design "C(90°)" (a variation of high-pass type), discussed in [17]. The two PTFE-based resonators differ in the width of the legs, which should bring different impedance of the resonator (at the resonance frequency), and, subsequently the different electric field strength (as described in [15] for resonators with lumped SMD capacitors).

Prior to fabrication, the resonators' designs were analyzed in Ansys HFSS software. The diameter and height of the resonators were fixed to 60 and 56 mm respectively. The width of the endrings (ER) was chosen as 6 mm for PI sub-

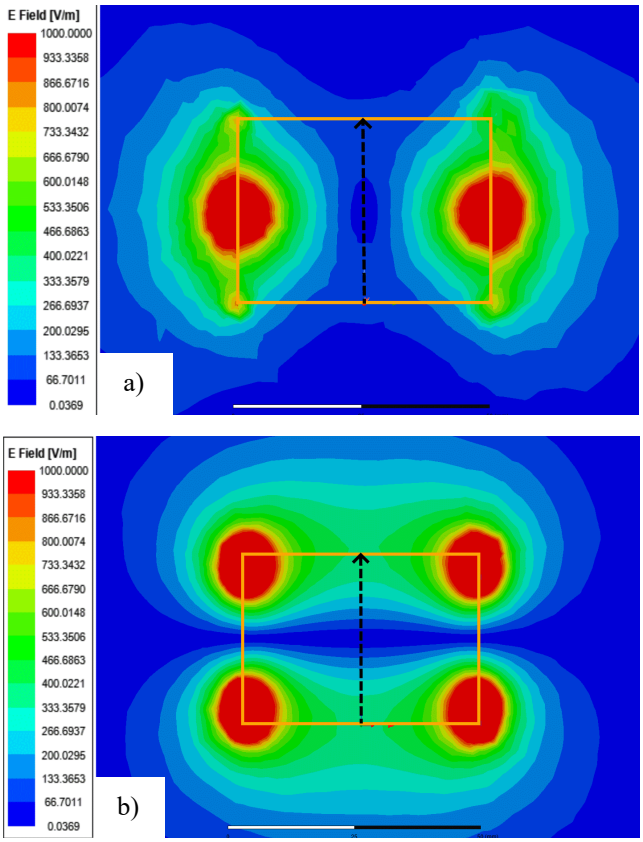

Fig. 3. E field distribution in a) low-pass and b) high-pass birdcage resonator. Adapted from [15] and modified.

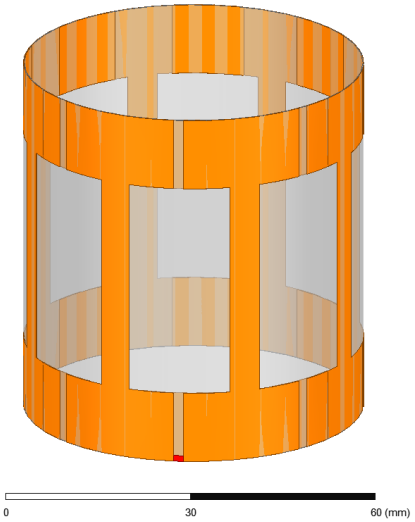

Fig. 4. Resonator PT-5.

strate and 12 mm for PTFE substrate (to partially compensate the different thickness and permittivity of the substrates). The leg width was chosen as 5 and 12 mm for both PTFE resonators. Finally, the length of the inner segment (as shown in Fig. 4) of the resonators was calculated in Ansys HFSS software. The fields' distributions were calculated for all resonance modes (see the modes in e.g., Fig. 5), and the fundamental resonance mode (the mode of our interest, which provides the homogeneous magnetic field and partially homogeneous electric field inside the resonator) was determined. Then, the length was swept, and its value was chosen, when the maximum of the impedance at the fundamental resonance mode was at the frequency close to 433 MHz.

For the purposes of this article, the resonators are named PI-5 (for Polyimide substrate) and PT-5 and PT-12 (for PTFE). The fourth resonator (named L) was only simulated to relate the capacity of the PT-12 resonator to the lumped-element equivalent. It shares the same geometry (diameter, height, and leg width), but the capacity is realized using lumped capacitors (Lumped RLC boundary in Ansys HFSS). The required capacity to keep the resonance frequency of the fundamental resonance mode at 433 MHz was 5.6 pF. The parameters of the resonators are listed in Tab. 1. Resonator PT-5 is also shown in Fig. 4.

Resonators were realized on the flexible substrate with copper foil on both sides. The substrate was chemically cleaned and preheated for good adhesion. The negative dry film photoresist was laminated on both sides. The negative resonator patterns were exposed to UV light (400 nanometers wavelength) on both sides. Exposed and unexposed areas have different solubility in the water-based solvent with sodium carbonate (1 % by wt). This developing process created a relief image of the master pattern. The ecological etchant of the solution of hydrochloric acid and hydrogen peroxide removed exposed (the nonsolid photoresist protected) copper foil. The polymerized photoresist was stripped in water solvent with sodium hydroxide and after final rinsing and drying the resonator master pattern was prepared.

	PI-5	PT-5	PT-12	L
Leg width (mm)	5.0	5.0	12.0	12.0
ER width (mm)	6.0	12.0	12.0	12.0
Length of outer ER seg. (mm)	20.1	20.5	20.5	N/A
Length of inner ER seg. (mm)	7.4	15.0	12.0	N/A

Tab. 1. Geometrical parameters of the resonators.

Finally, an RG-316 coaxial cable was soldered between two of the adjacent endrings segments and the cable was terminated with an SMA connector (therefore, the connection corresponds to the lumped port position highlighted by red color in Fig. 4).

3. Characterization of the Resonators

The resonators were analyzed in Ansys HFSS. From the analysis, the maximal value of the real part of the impedance at the resonance frequency at the fundamental resonance mode (around 433 MHz) was extracted. Also, the electric and magnetic field strength along the resonator's axis was obtained. The parameters of the fabricated resonators were measured using a vector network analyzer (VNA) Rohde & Schwarz ZVL 9 kHz–6 GHz and their impedance was calculated from the reflection coefficient (S_{11}). From the simulated and measured curves of impedance, the Q factor was extracted. The Q factor was calculated as a ratio of the resonance frequency and the frequency bandwidth, where the impedance is higher than the peak impedance divided by square root of two.

Both simulated and measured impedance curves show, that the highest peak impedance is obtained with resonator PT-5 (Fig. 5), followed by PT-12 (Fig. 6) and the peak impedance is lowest with resonator PI-5 (Fig. 7). The maximal (peak) values are shown in Tab. 1. Although the figures create a clear overview of the impedance of the resonators, the maximal values were extracted from the more detailed sweep and measurement with higher frequency resolution.

	PT-5	PT-12	PI-5
f sim. (MHz)	434.3	433.2	434.7
f ms. (MHz)	425.7	425.1	425.3
Re sim. imp. (Ω)	644.3	537.6	487.3
Re ms. imp. (Ω)	697.0	599.9	545.7
Q sim.	102.0	106.2	58.4
Q ms.	145.7	141.7	94.5
E_{max} sim. (V/m)	799.5	715.3	599.8
H_{max} sim. (V/m)	10.46	12.48	8.97

Tab. 1. Simulated (sim.) and measured (ms.) electrical parameters of the fabricated resonators.

The electric and magnetic fields inside the resonators are shown in Fig. 8 and Fig. 9, respectively. The electric field is displayed at initial phase 0°, while the magnetic field at phase 90° (with the power of excitation 1 W). The maximal values are also written in Tab. 1. The electric field is highest for resonator PT-5 and lowest for PI-5. On the other hand, the magnetic field inside the resonator is highest for the resonator PT-12 and lowest for PI-5. Q factors calculated

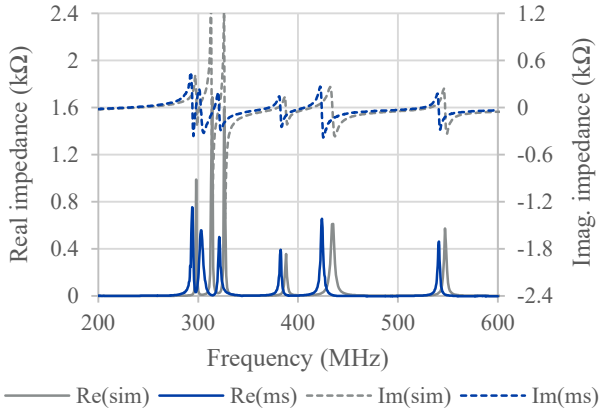

Fig. 5. Results of simulation (sim) and measurement (ms) of real and imaginary part of impedance of the resonator PT-5.

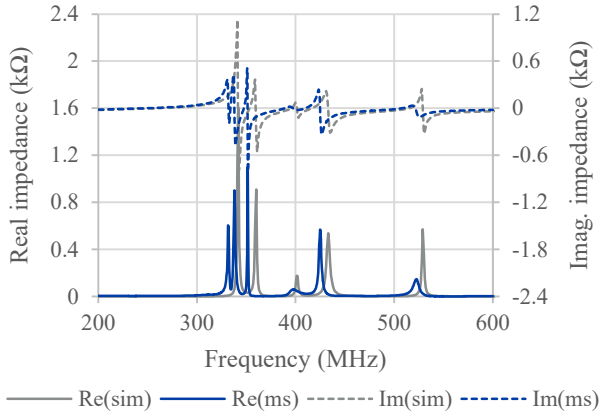

Fig. 6. Results of simulation (sim) and measurement (ms) of real and imaginary part of impedance of the resonator PT-12.

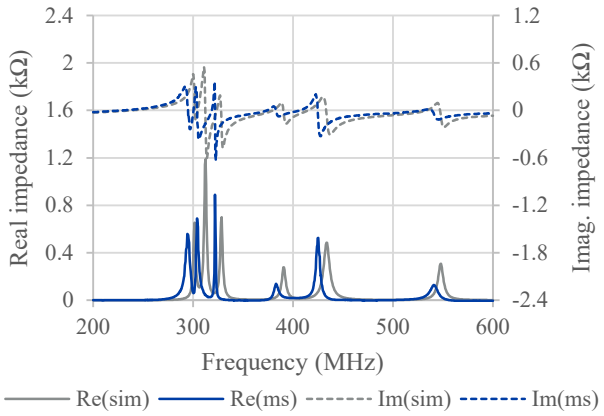

Fig. 7. Results of simulation (sim) and measurement (ms) of real and imaginary part of impedance of the resonator PI-5.

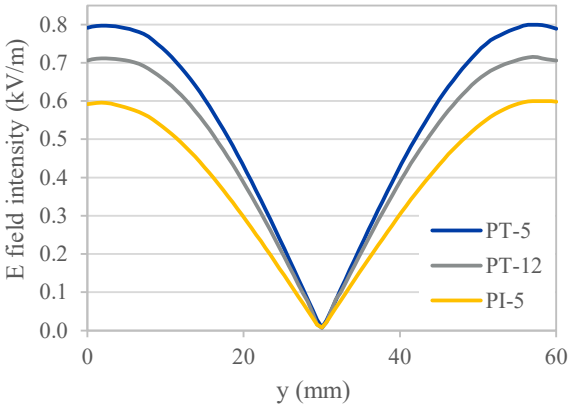

Fig. 8. Electric field strength along the resonators' axis (simulated using Ansys HFSS).

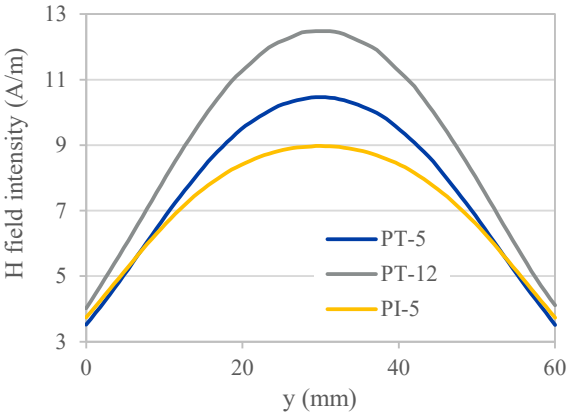

Fig. 9. Magnetic field strength along the resonators' axis at 90° phase (simulated using Ansys HFSS).

from both the simulated and measured curves are also listed in Tab. 1.

The higher the impedance of the resonators at the resonance frequency, the higher the electric field, which the resonators create. This is in accordance with our previous findings [15] with lumped-element equivalents. A more complicated situation occurs with the magnetic field strength. The resonator PT-12 creates the magnetic field of higher strength than the resonator PT-5. However, resonator PI-5 creates the lowest strength of the magnetic field of all three. This may imply, that there are higher losses in polyimide material, compared to the PTFE. This is also supported by both measured and simulated Q factors. While both PT resonators' behavior is almost the same, the Q factor of the PI resonator is significantly lower. The measured values (peak impedance and Q factor) are higher than the simulated ones. This might be explained by the high uncertainty of measurement of high impedance by a VNA, or by the non-ideal material database in Ansys HFSS. However, besides this error, the ratios of these values are similar for both simulation and measurement.

4. Plasma Excitation

For tests in a real environment of the plasma excitation, the resonators were connected to our plasma apparatus. The

apparatus consists of a discharge channel (where the resonators were placed on) created from Pyrex glass, vacuum system (the pressure was kept in the range from 0.984 to 0.986 Pa, with a 1% error of the pressure gauge) and a pair of coils for static magnetic field excitation. The direct current in the coils was set to create the static magnetic field in the range of tens of militesla, to magnetically confine the plasma inside the discharge channel (the current was kept constant during the whole experimental procedure, however, the specific value is not crucial, since we want only to compare the prepared resonators, and the static magnetic field optimization will be done further in the future).

Then, the resonators were matched to 50 Ω by placing a microwave air variable capacitor in series. Matching was proceeded with respect to minimal power reflection, which was monitored as S_{11} signal using VNA R&S ZVL (9 kHz to 6 GHz). Then, the resonators were connected to an RF power source (consisting of a signal generator Rohde & Schwarz SMC100A, an amplifier and a circulator for protection in case of high power reflection). Fine-tuning of the matching was done when the resonators were connected to the power source, to decrease the reflected power (which was monitored at the third port of the circulator using spectrum analyzer Agilent N9320A) to a minimal value. The final frequency of operation was found to be 416.65 MHz for PT-5, 418.00 MHz for PT-12 and 417.52 MHz for PI-5.

When the pressure in the apparatus stabilized, the input power was raised until a discharge occurred. Followingly, the input power was decreased until the discharge was extinguished. The whole process was repeated several (fifteen to twenty) times and the lowest power when the discharge ignites or sustains was recorded and is shown in Tab. 2. The exact level of incident power was measured with spectrum analyzer Agilent N9320A. At the incident power level of ignition, also the reflected power was monitored (to ensure the sufficient power absorption), however, without the static magnetic field, therefore without the discharge inside the resonator. The reflected power was lower than 10 mW at the power level used for PT-5 excitation and lower than 30 mW at the power levels used for PT-12 and PI-5. Conclusively, the best results were achieved with resonator PT-5, which was able to form a discharge with the lowest incident power.

The performance in plasma excitation follows the trend of measured impedances and electric fields inside the resonator. A resonator, which is able to excite a higher electric field with constant input power, will be able to ignite the discharge at lower power levels.

	PT-5	PT-12	PI-5
Power level of plasma ignition (W)	0.34	1.03	1.49
Power level of plasma sustainment (W)	0.16	0.43	0.57

Tab. 2. The lowest excitation power (forward power), at which the plasma was ignited and sustained.

5. Impedance Matching

The resonators were matched by a capacitor in series, during the experiments. Although this way of matching is the most straightforward, the more advanced means of matching are often used. For example, in [9], there is stated: "The dominantly real input impedance near to antenna resonance avoids the problem of strong reactive currents and voltages in the matching box and RF power connections." Such a statement suggests that the matching with a capacitor in series probably was not used.

To examine, if the capacitive matching in series could have any significant impact on the performance of the resonators (or on the final plasma source respectively), the numerical model of the best-performing resonator (PT-5) was adjusted. The impedance of the lumped port was set to 50 Ω, and at one side of the lumped port, between the port and the body of the resonator, the Lumped RLC boundary condition was added. An ideal capacitor was considered, therefore only the capacity was set to a certain value. The value was chosen to achieve the minimal power reflection (–34 dBm) when the real part of the impedance of the resonator equals 50 Ω. The comparison of the electric field (the field was extracted at the point at the axis of the resonator, 3 mm from its edge) of such a matched resonator with the resonator with theoretical ideal matching (the impedance of the lumped port was set the same as the impedance of the resonator at the resonance frequency) is shown in Fig. 10. For clarity, also the S_{11} curves are depicted.

Figure 10 shows that the ideal peak matching can bring much better results, than matching the resonator in series with an ideal capacitor. The maximum electric field is significantly higher, moreover, the maximum electric field strength lies at the exact same frequency as the minimum of S_{11} curve. The highest portion of the incident power can, therefore, be exploited. However, these results are valid only for a case of an ideal matching network and do not consider the practical aspect of the real samples.

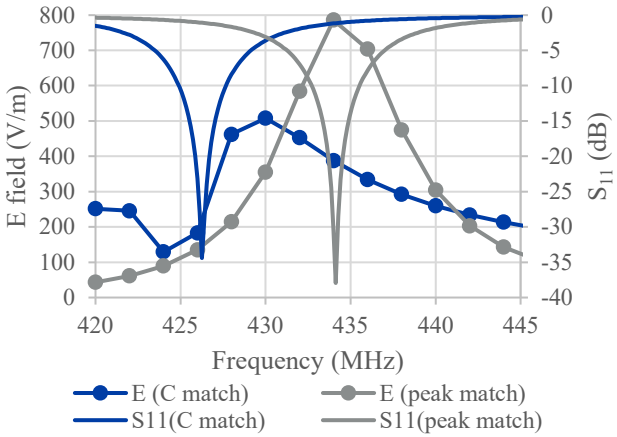

Fig. 10. Comparison of electric field strength for ideal peak matching and series capacitive matching (simulated in Ansys HFSS).

To compare the real matching in the real application case, the resonator PT-5 was further tested with an inductive matching. A coupling loop, with the inner dimensions the same, as the inner dimensions of a loop created by two adjacent resonator legs was created of 12 mm wide copper tape. The loop was soldered together from the individual pieces of the tape, and an SMA connector, in series with the variable capacitor, was added. Then, the optimal distance was set, between the resonator placed on the apparatus and the coupling loop, to keep the real part at the top of the resonance peak at 50 Ω and the variable capacitor was adjusted to set the imaginary part of the impedance to 0 Ω. Then, the same experiment as described in Sec. 4 was repeated.

With the inductive coupling loop, the resonator's performance was poorer than with the capacitive series matching. The resonance frequency, in this case, was 421.06 MHz (the static magnetic field was adjusted to the frequency change). The lowest power required for a discharge ignition was 0.49 W, while it was possible to sustain the discharge at the power of 0.26 W (compare with 0.34 W and 0.16 W respectively for series capacitive matching).

To test the performance that will be available in a real application, a simple apparatus for ion extraction was created. An extraction grid was placed 10 mm apart from one of the endrings. The discharge channel was terminated by a stainless-steel cone, which was located 150 mm away in the same direction as the extraction grid. Schematic drawing of the apparatus is shown in Fig. 11. Between the extraction grid and the collector, a voltage of 120 V was imposed (with negative voltage at the collector). The current between these two electrodes was measured using a digital multimeter Agilent 34410A. The measured current was 22.05 μA for capacitive serial matching and 11.18 μA for inductive matching (with an error of the multimeter lower than 0.01 μA). The measurement of the extracted current was done at the same input power level for both channels (12.9 W).

The impact of different power coupling is probably much lower than the added power losses for the inductive power transfer from a coupling loop to the resonator. Part of the RF power probably dissipated in the surrounding segments of the apparatus as well. Although it might be interesting to study the impact of other means of impedance matching with regards to theoretically achievable electric field strength and homogeneity, for practical application in plasma source engineering, even the simplest matching with a capacitor connected in series is sufficient.

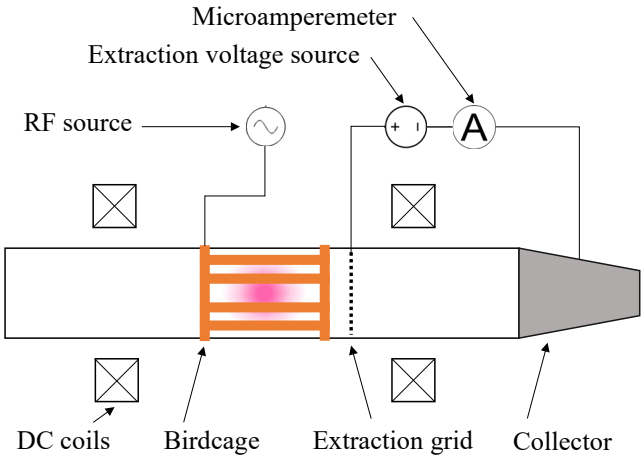

Fig. 11. Schematic drawing of the apparatus.

6. Conclusion

The deviation of the resonance frequency of the fabricated sample compared to the simulations is only 2.2% for the worst resonator. Therefore, the described approach is reliable to use for different resonators' design as well as for the different materials of the substrate. The plasma excitation performance as well as the electrical parameters are stably changed across the resonators, which can help to predict the performance of other resonators in the future. The best-performing resonator is also working well within the plasma source, where only 0.34 W of input power is needed to ignite the discharge.

There is a space for optimization of the described plasma source, such as the optimization of position, shape and strength of static magnetic field or the geometry of current-extraction probe. However, the scope of this paper was only to describe and present the fabrication of the resonators and compare the influence of the individual parameters on the resulting performance. The optimization of the other parts of the plasma source will be done in future, which will bring even better results, especially with respect to the pressure level in the apparatus and the extracted ion current.

Acknowledgments

This work has been supported by grant FEKT-K-22-7732 realized within the project Quality Internal Grants of BUT (KInG BUT), Reg. No. CZ.02.2.69 / 0.0 / 0.0 / 19_073 / 0016948, which is financed from the OP RDE.

References

[1] HAYES, C. E., EDELSTEIN, W. A., SCHENCK, J. F., et al. An efficient, highly homogeneous radiofrequency coil for whole-body NMR imaging at 1.5 T. *Journal of Magnetic Resonance (1969)*, 1985, vol. 63 no. 3, p. 622–628. DOI: 10.1016/0022-2364(85)90257-4

[2] PASCONE R. J., GARCIA, B. J., FITZGERALD T. M., et al. Generalized electrical analysis of low-pass and high-pass birdcage resonators. *Magnetic Resonance Imaging,* 1991, vol. 9, no. 3, p. 395–408. DOI: 10.1016/0730-725X(91)90428-O

[3] HAYES, C. E. The development of the birdcage resonator: A historical perspective. *NMR in Biomedicine*, 2009, vol. 22, no. 9. p. 908–918. DOI: 10.1002/nbm.1431

[4] FANTASIA, M., GALANTE, A., MAGGIORELLI, F., et al. Numerical and workbench design of 2.35 T double-tuned ($^{1}H/^{23}Na$) nested RF birdcage coils suitable for animal size MRI. *IEEE Transactions on Medical Imaging,* 2020, vol. 39, no. 10, p. 3175 to 3186. DOI: 10.1109/TMI.2020.2988599

[5] SON, H., AHMAD, S. F., CHOI, J., et al. Effect of distributed capacitance on the performance of birdcage type RF coil for 1 H MRI. In *Proceedings of the International Symposium on Antennas and Propagation*. Jeju (Korea), 2011, p. 52–58.

[6] KRIEGL-FRASS, R., NAVARRO DE LARA, L. I., PICHLER, M., et al. Flexible 23-channel coil array for high-resolution magnetic resonance imaging at 3 Tesla. *PLoS One*, Nov. 2018, vol. 13, no. 11, e0206963. DOI: 10.1371/journal.pone.0206963

[7] VÍT, M., BURIAN M., BERKOVÁ, Z., et al. A broad tuneable birdcage coil for mouse 1H/19F MR applications. *Journal of Magnetic Resonance*, 2021, vol. 329, p. 1–10. DOI: 10.1016/j.jmr.2021.107023

[8] AHMAD, S. F., KIM, Y. C., CHOI, I. C., et al. Recent progress in birdcage RF coil technology for MRI system. *Diagnostics*, 2020, vol. 10, no. 12, p. 1–19. DOI: 10.3390/diagnostics10121017

[9] GUITTIENNE, P., CHEVALIER, E., HOLLENSTEIN, C. Towards an optimal antenna for helicon waves excitation. *Journal of Applied Physics*, 2005, vol. 98, no. 8, p. 1–6. DOI: 10.1063/1.2081107

[10] GUITTIENNE, P., HOWLING, A. A., HOLLENSTEIN, C. Analysis of resonant planar dissipative network antennas for rf inductively coupled plasma sources. *Plasma Sources Science and Technology*, 2014, vol. 23, no. 1, p. 1–13. DOI: 10.1088/0963-0252/23/1/015006

[11] HOWLING, A. A., GUITTIENNE, P., JACQUIER, R., et al. Complex image method for RF antenna-plasma inductive coupling calculation in planar geometry. Part I: Basic concepts. *Plasma Sources Science and Technology*, 2015, vol. 24, no. 6, p. 1–8. DOI: 10.1088/0963-0252/24/6/065014

[12] GUITTIENNE, P., JACQUIER, R., POURADIER, B., et al. Helicon wave plasma generated by a resonant birdcage antenna: Magnetic field measurements and analysis in the RAID linear device. *Plasma Sources Science and Technology*, 2021, vol. 30, no. 7, p. 1–14. DOI: 10.1088/1361-6595/ac0da3

[13] SEO, J. H., CHUNG, J. Y. A preliminary study for reference RF coil at 11.7 T MRI: Based on electromagnetic field simulation of hybrid-BC RF coil according to diameter and length at 3.0, 7.0 and 11.7 T. *Sensors*, Feb. 2022, vol. 22, no. 4, p. 1–26. DOI: 10.3390/s22041512

[14] SEO, J.-H., HAN, Y., CHUNG, J.-Y. A comparative study of birdcage RF coil configurations for ultra-high field magnetic resonance imaging. *Sensors*, Feb. 2022, vol. 22, no. 5, p. 1741 to 1760. DOI: 10.3390/s22051741

[15] JURIK, K., DREXLER, P., NESPOR, D., et al. Parametric optimization of a birdcage resonator for low-pressure plasma excitation. In *Progress in Electromagnetics Research Symposium (PIERS)*. Hangzhou (China), 2021, p. 455–461. DOI: 10.1109/PIERS53385.2021.9694714

[16] JURIK, K., DREXLER, P. Design and numerical analysis of a birdcage resonator without lumped capacitors. In *3rd URSI Atlantic and Asia Pacific Radio Science Meeting (AT-AP-RASC)*. Gran Canaria (Spain), 2022 p. 1–2. DOI: 10.23919/AT-AP-RASC54737.2022.9814355

[17] JURIK, K., DREXLER, P. Tubular resonant networks creating a homogeneous magnetic field via different resonance modes. In *Mediterranean Microwave Symposium (MMS)*. Pizzo Calabro (Italy), 2022, p. 1–4. DOI: 10.1109/MMS55062.2022.9825529

About the Authors …

Karel JUŘÍK (corresponding author) was born in 1996 in Boskovice. He graduated from Brno University of Technology in 2020, where he is currently enrolled as a PhD student. His research interests include scientific instrumentation, specifically electromagnetic resonators, and their application in rf-driven plasma sources.

Jiří STARÝ was born in 1957. After Brno University of Technology graduation in 1982, he was working in research and development in the electronic factory Tesla Brno for 10 years. His main focus at Brno University of Technology is oriented to the technology of printed circuit boards and surface mount assembly techniques, mainly soldering processes.

Petr DREXLER, born in 1980, graduated from Brno University of Technology in 2004 where he also received his Ph.D in Electrical Engineering in 2007. His scientific interest comprises the research of functional electromagnetic structures and devices for the sensing application and diagnostics of phenomena in electromagnetic fields and signals.